# Low-Threshold Continuous-Wave Operation of Electrically Pumped 1.55 μm InAs Quantum Dash Microring Lasers
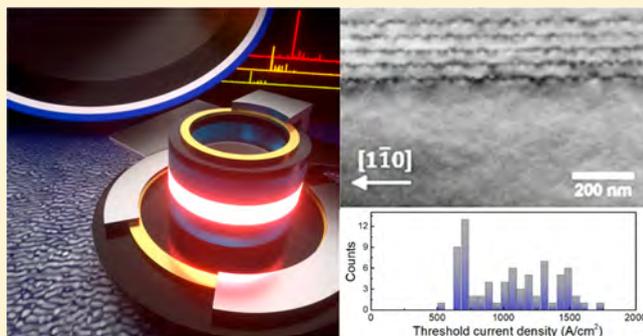
Yating Wan,*[†,‡] Daehwan Jung,[†,‡] Chen Shang,[‡,§] Noelle Collins,[∥] Ian MacFarlane,[∥] Justin Norman,[§] Mario Dumont,[∥] Arthur C. Gossard,[†,§,∥] and John E. Bowers[†,§,∥]

[†]Institute for Energy Efficiency, [§]Materials Department, and [∥]Department of Electrical and Computer Engineering, University of California Santa Barbara, Santa Barbara, California 93106, United States

**ABSTRACT:** Densely integrated devices on a single chip enable both complex functionality and economy of scale. With a small footprint, microcavities with self-assembled InAs quantum dashes (QDashes) use minimal real estate cost while offering full photonic functionality. Here, the first room-temperature-continuous-wave (CW) operation of electrically pumped InAs QDash microring lasers in the 1.55 μm telecom window is reported. CW lasing up to 55 °C has been achieved with a low threshold current density of 528 A/cm². The ring laser has only a few unique modes with an extinction ratio over 26 dB for the primary mode. The reduced carrier diffusion length of the QDash active region suppresses the sidewall surface recombination. Feasibility of device minia-turization was demonstrated, with the lowest threshold being 3.5 mA. Since microring cavities do not require feedback mirrors, their compact size and resulting low thresholds make them the ideal candidate for an on-chip light source in optical datacom interconnects.

**KEYWORDS:** *quantum dashes, low threshold, microring lasers, C-band communication, photonic integrated circuits*

Following a photonic Moore's law, there is a need to minimize the size and power consumption of microlasers to enable an increase in both complexity and functionality of photonic integrated circuits.[1] Microring lasers, with total internal reflection of light traveling at the periphery of the resonator, are typically more compact than conventional linear planar cavity lasers, such as Fabry–Perot (FP), distributed Bragg reflector (DBR), and distributed feedback (DFB) lasers.[2] The compact size of microring lasers results in low threshold, single mode operation and high direct modulation speed.[3] The whispering gallery mode (WGM) operation requires no cleaved facets, wavelength-selective gratings, or reflective coatings for optical feedback. This offers a monolithic solution for in-plane photonic circuit integration.[4] However, strong nonradiative surface recombination at microresonator sidewalls becomes an issue as the resonator size is reduced to tens of microns. In the first demonstration of 1.55 μm microdisk injection laser,[5] the sidewall exposure of the active layer in the microcavity lasers resulted in high thresholds and rapid device degradation. Typically, the lifetime was only a few hours, with a noticeable decrease in the output power.[6]

To minimize the nonradiative recombination on the resonator surface and to achieve ultralow threshold lasing in small volume cavities, the use of quantum dots (QDs) instead of quantum wells (QWs) as the active medium has been actively investigated.[7] To date, exceptional microcavity laser performance based on InAs/GaAs QDs has been achieved in

the 1.3 μm band, with a sub-mA threshold current,[8] subwavelength optical cavities,[9,10] and high temperature stability.[11,12] However, it is challenging to extend the emission wavelength of these GaAs-based lasers to 1.55 μm without using metamorphic buffers, which typically results in high threshold current densities and severe lifetime degradation.[13] The 1.55 μm emission from InAs quantum dashes (QDashes) grown on InP substrates can be easily achieved as the lattice mismatch between InAs and InP is smaller (3.2%).[14] Since the first demonstration of self-assembled InAs QDash lasers grown on InP (001),[15,16] substantial improvement in device characteristics has been made in recent years.[14,17] The best value of threshold current density of 730 A/cm² (46 A/cm² per layer)[18] and 540 A/cm² (108 A/cm² per layer)[19] has been achieved. Interesting phenomena, such as excitonic emission from a single Qdash,[20] optical bistability and nonlinear switching,[21] have been investigated. By exploiting the inherent inhomogeneous nature and ultrabroad gain profile of Qdashes, highly attractive broadband optical components have been made.[22,23] In this field of study, broadband optical amplifiers,[24,25] mode-locked lasers,[26,27] and superluminescent diodes[22] are three examples of the recent significant developments. Nevertheless, the use of 1.55 μm QDash material for microring lasers has been relatively unexplored to date. There

are few results in large (millimeter-length) ring lasers,[28,29] typically with a high threshold current density of 6.4 kA/cm$^2$ at near room temperature (283 K).[30] Recently, 1.55 $\mu$m InAs/InAlGaAs QD microdisk lasers have been demonstrated with a low threshold power of 1.6 mW under continuous optical pumping.[31] However, electrical injection of this type of laser is still in its infancy. Improved current injection is needed, as well as fabrication of small and low-resistance contacts that do not significantly perturb the optical cavity.

In this Letter, we demonstrate high-performance InAs QDash microring lasers in the 1.55 $\mu$m telecom window under continuous electrical injection. The InAs QDashes employed in these lasers undergo a growth interruption process to ripen InAs nanostructures, which enhanced their optical properties.[32] A WGM ring cavity with vertical etched profile and smooth sidewall surface was fabricated, allowing strong lateral optical confinement and low scattering losses. Continuous-wave (CW) lasing up to 55 °C with a low threshold current density of 528 A/cm$^2$ has been achieved for a microring laser with a ring radius ($R$) of 100 $\mu$m. For smaller devices ($R$ = 30 $\mu$m) with a larger free spectral range (FSR), single-mode operation was observed with extinction ratio over 26 dB in 1.55 $\mu$m.

Samples were grown by solid-source molecular beam epitaxy. Photoluminescence (PL) samples with one QDash layer surrounded by InAlGaAs matrix lattice-matched to InP were grown to study their optical properties. The QDash layers are composed of 3.75 ML of InAs grown at 500 °C and were measured by optical pyrometer. After QDashes were formed, growth was paused under As$_2$ overpressure for a 60 s ripening period.[32] Figure 1 shows the room-temperature PL spectrum
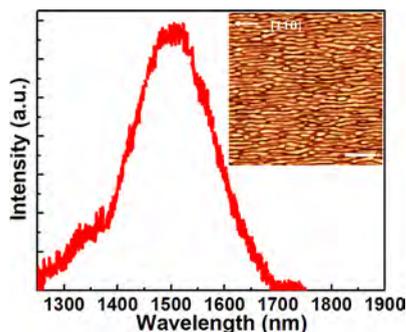


**Figure 1.** Photoluminescence spectrum of the as-grown sample. Inset: atomic force microscopy image of QDashes with a density of 1.3 × 10$^{10}$ cm$^{-2}$. The scale bar is 200 nm.

with a ground-state emission at 1500 nm and a full-width-at-half-maximum (fwhm) of 98 meV. QDashes elongated along the [1$\bar{1}$0] direction were observed with atomic force microscopy, as shown in the inset of Figure 1, and the density was measured to be 1.3 × 10$^{10}$ cm$^2$.

The full laser structure is schematically shown in Figure 2. The $n$- and $p$-type InAlAs cladding layers, lattice-matched to InP, were used for transverse optical confinement. The 100 nm thick InAlGaAs digital alloys with alternating lattice-matched InAlAs/InGaAs layers were grown to form a separate-confinement heterostructure (SCH). A 200 nm thick $p$-doped InGaAs layer was finally deposited as the $p$-contact layer. The cross-sectional bright-field transmission electron microscopy (TEM) image in Figure 2 reveals the coherent five QDash layers under the **g** = (002) two-beam condition. The

as-grown material was processed into ring-waveguide lasers with radii ranging from 25 to 100 $\mu$m and ring widths of 4 $\mu$m. To maximize the optical confinement mode and minimize current spreading, the ring waveguides were deeply etched through the active core layer.

It is noted that optical scattering from sidewalls as well as carrier surface recombination are two major limiting factors in the performance of deeply etched structures. The reduced carrier diffusion length of the QDash active region suppresses the sidewall surface recombination. Additionally, the fabrication parameters have been carefully optimized for the inductively coupled plasma (ICP) etch to achieve vertical and smooth sidewalls. The chamber pressure was maintained at 1.4 mTorr, with the coil and plate power set as 800 and 125 W, respectively. Cl$_2$, H$_2$, and Ar mixed gases were used with flow rates of 6.3, 12.7, and 2 sccm, respectively. The chamber temperature was set at 200 °C, with thermally conductive glue applied on the back of the wafers to provide good thermal conductance between the chuck and the wafer. After etching, the sidewall was passivated with 12 nm of Al$_2$O$_3$ by atomic-layer deposition (ALD). The pinhole-free and conformal Al$_2$O$_3$ deposition provides excellent surface passivation,[33] which shows improved photoluminescence efficiency in InP nanowires[34] and reduced scattering loss in InGaAsP photonic-wire waveguides[35] in literature. A 1 $\mu$m thick SiO$_2$ layer was then sputtered to fully isolate the optical modes from the Pd/Ti/Pd/Au and Pd/Ge/Pd/Au metal contact stacks. Top-view and cross-sectional scanning electron microscope (SEM) images of a fabricated device are shown in Figure 3.

The output power was measured by capturing the radiation out-coupling from the ring cavity by an integrating sphere placed 5 mm from the ring cavity edge. A ~90° azimuthal light-radiation-collection angle was estimated for such a geometry. Considering the angular directivity pattern of radiation and the detector's spectral sensitivity, the optical power magnitude (0.18 mW at an injection current of 80 mA) presented here is an underestimate. Figure 4a shows the light−current−voltage (L-I-V) characteristics of a representative ring laser of outer $R$ 100 $\mu$m and ring width ($W$) 4 $\mu$m, with a threshold current ($I_{th}$) of 13 mA. A logarithmic plot of the LI curve is presented in the inset in Figure 4a, exhibiting an "S-shaped" nonlinear transition from spontaneous emission to stimulated emission. CW operation with no sign of performance degradation and power roll-off was observed up to injection current values as high as 5× the threshold. The corresponding threshold current density $J_{th}$ has an ultralow value of 528 A/cm$^2$, which indicates excellent nonradiative recombination suppression at the deeply etched sidewalls of the Qdash structures.

The spectra shown in Figure 4b were measured by coupling output light into a lensed fiber connected to an optical spectrum analyzer. Only a few unique modes with spectrally distant spacing were observed. This is most likely caused by relatively few WGMs falling within the gain spectrum of the QDashes. Due to the different overlap of WGMs with the QDashes, each WGM can have different quality factors and different susceptibility to defects and imperfections. Here, an extinction ratio over 26 dB was observed for the primary lasing mode at ~1530 nm near the PL intensity maximum of the ground-state optical transition in QDashes, due to the advantages in spatial overlapping of emitters to the surrounding cavity, radiative emission rate, or resonance in frequency.[10] The peak at 1550 nm was plotted separately in
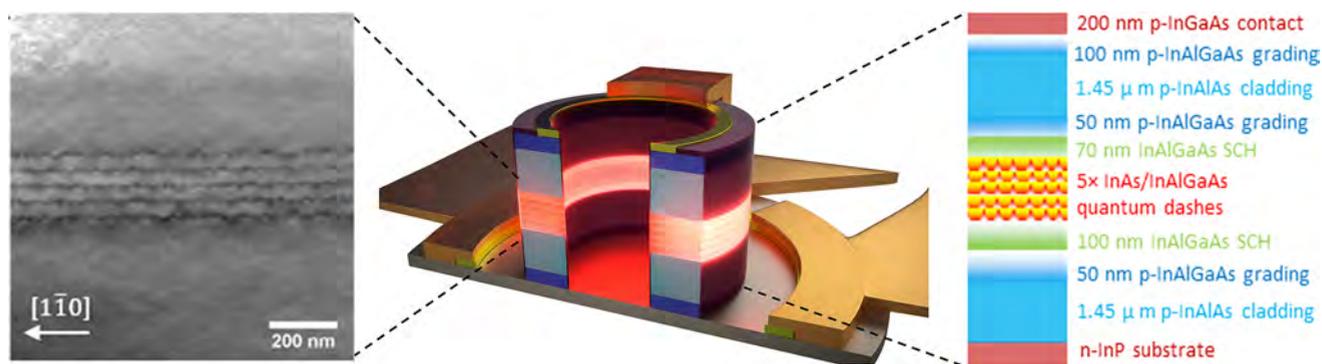
**Figure 2.** Schematic diagram of the fabricated microring laser epilayer structure and cross-sectional transmission electron microscopy image in the QDash active region.
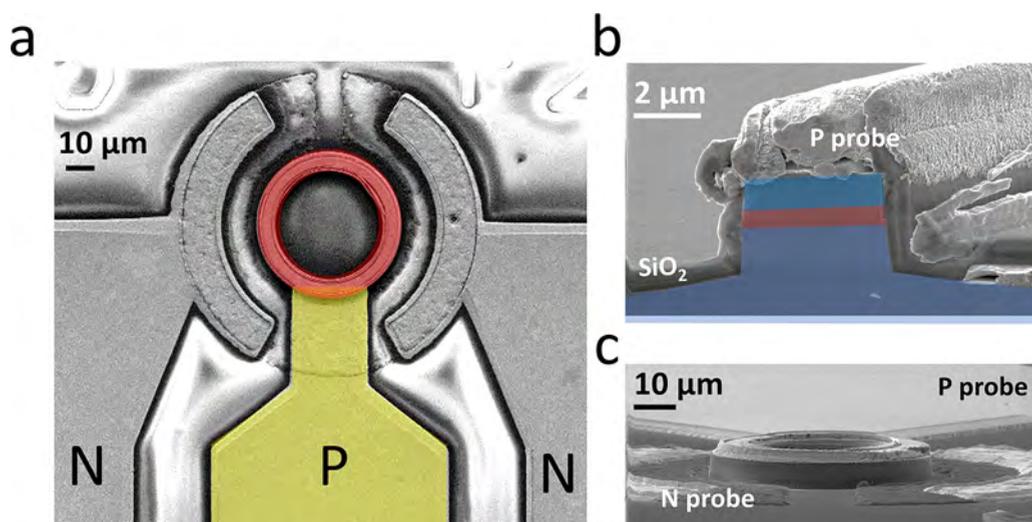


**Figure 3.** SEM images of the fabricated device. Top-view (a) and cross-sectional views (b) of a fabricated microring laser (c). Highlighted color sections: red, microring laser (a) and active region (b); blue, III−V; yellow, selected metal contacts.

Figure 4c, and the fine mode spacing was measured to be ~1.06 nm. The group refractive index of the cavity was calculated to be 3.6 accordingly. Consistent single-wavelength lasing has been observed in 80 $\mu$m and smaller diameter devices with larger FSRs. A side-mode suppression ratio of 9 dB was observed for an 80 $\mu$m diameter device at an injection current of 40 mA (Figure 5).

The extracted central wavelengths of the two primary modes are plotted as a function of injection currents in Figure 4d. The red shift of wavelengths (0.207 nm/mA for mode at ~1550 and 0.202 nm/mA for mode at ~1530 nm) with the increase of bias current was observed due to laser self-heating. The slope of dissipated electric power was 0.094 nm/mW accordingly. Figure 4e shows the wavelength temperature dependence of laser modes at a fixed injection current of 50 mA. With increasing temperature, the spectral position of the modes slightly shifts by ~0.12 nm/°C; this is due to the temperature dependence of the refractive index. Therefore, microring laser self-heating at threshold is around 22 °C. Thermal impedance of the device $R_T = (d\lambda/dP)/(d\lambda/dT)$ was calculated to be 0.78 °C/mW, accordingly. This value is comparable to the state-of-art 1.3 $\mu$m InAs QD microdisk lasers[11] and can be reduced by using a benzocyclobutene planarization layer.[36]

High-temperature CW operation of the same device ($r$ = 100 $\mu$m, $w$ = 4 $\mu$m) was demonstrated up to 55 °C.

Temperature-dependent lasing of this device is shown in Figure 6a. A plot of the CW threshold current versus the stage temperature for this device, along with three other lasers of various outer-ring radii, is shown in Figure 6b. The characteristic temperature $T_0$ was extracted by fitting the increase in threshold using an exponential function $I_{th}(T) \propto \exp(T/T_0)$ and found to be ~39 K. This is a record-high value for 1.55 $\mu$m microring QDash lasers. Note that the previous reported QD ring laser can only operate at near room temperature.[30] The inset in Figure 6b shows the extracted $T_0$ as a function of outer-ring radius. Decrease in the ring cavity size leads to a slight deterioration of the maximum operating temperature, decreasing from 55 to 50 °C when the outer-ring radius scales from 100 to 30 $\mu$m. $T_0$, however, stays almost constant in the range of 30−40 K. This suggests minimal increase of thermal resistance for smaller ring cavities.

A plot of the threshold current versus the outer ring radius for 74 lasers is shown in Figure 7a. The average threshold per ring size varies from 6.5 to 17 mA, and the spread in thresholds for each size is within 1.7 mA. Figure 7a shows the sharp decrease in threshold current with decreasing ring diameter, reaching a minimum of 3.5 mA. The observation of threshold reduction with cavity shrinkage demonstrates the suppression of nonradiative sidewall recombination. A histogram of the threshold current density for the above-mentioned devices is presented in Figure 7b, with a variation in threshold current
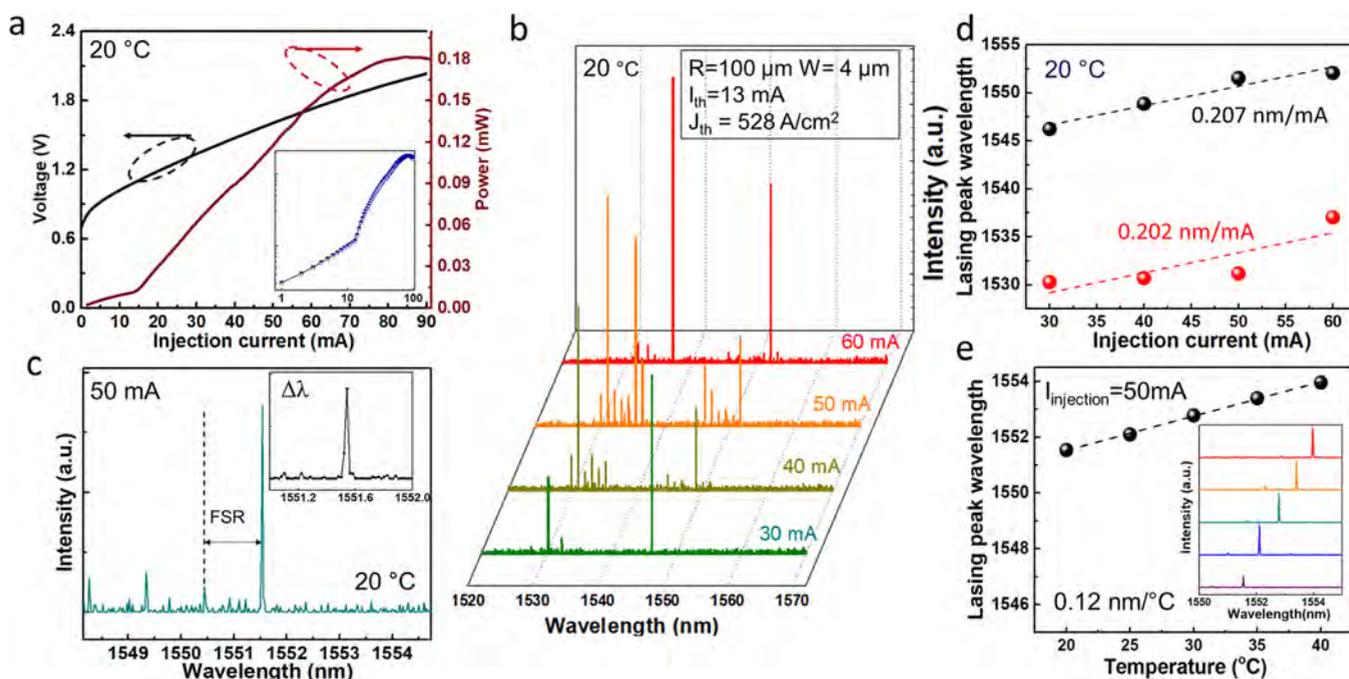
**Figure 4.** (a) Light−current−voltage characteristics, inset: LI curve in the log−log scale. (b) Emission spectra at increasing injection currents of a microring laser with a radius of 100 μm and a ring width of 4 μm under CW operation at room temperature. (c) Zoomed-in view of the spectrum taken at 50 mA. (d) Lasing wavelength as a function of injection current for the primary lasing modes at ∼1550 and ∼1530 nm and (e) temperature dependences of the laser mode wavelength at ∼1550 nm for the same device.
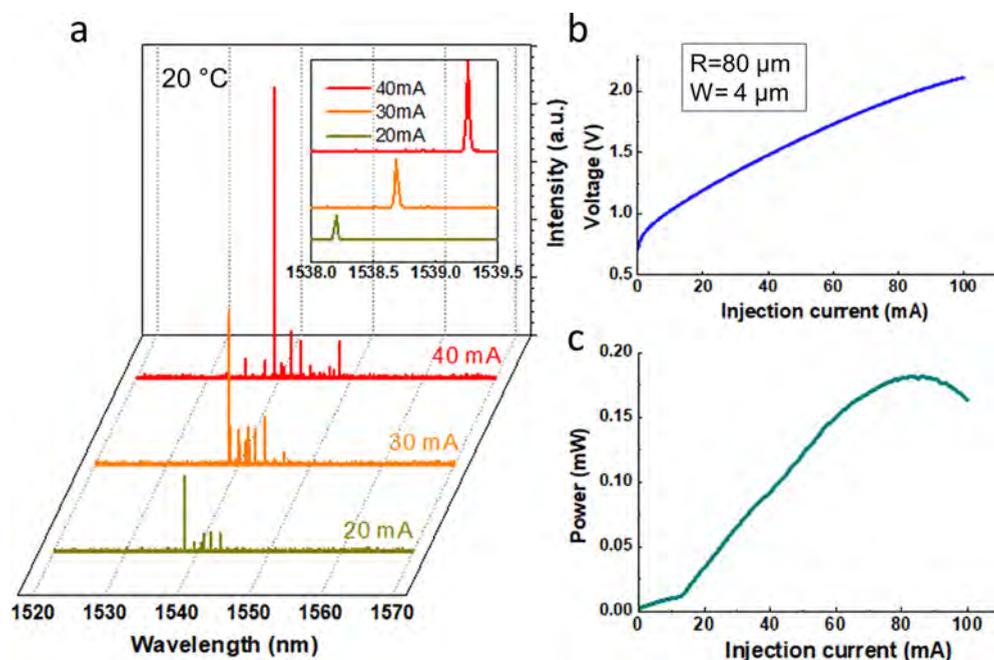


**Figure 5.** (a) Emission spectra at increasing injection currents of a microring laser with a radius of 80 μm and a ring width of 4 μm under CW operation at room temperature. Inset: Zoomed-in view of the spectra. (b, c) Light−current−voltage characteristics.

density from 528 to 1741 A/cm$^2$. This is attributed to the variation of surface roughness during the dry etching steps and overheating in devices with imperfect electrical contacts.

In summary, we presented record-high performance of 1.55 μm InAs/InAlGaAs QDash microring lasers epitaxially grown on InP (001) substrates. The self-assembled QDashes provide excellent carrier localization when compared to a two-dimensional QW structure. This reduces the device sensitivity to various thermally activated processes, such as carrier escape

from the active region and nonradiative recombination at the ring cavity side walls. Additionally, efficient device scaling to smaller footprints and lower power consumption have been demonstrated, with smallest threshold current of 3.5 mA, CW lasing up to 55 °C, and low threshold current density of 528A/cm$^2$. These results show promise for replacing the QWs in microemitters with QDashes in hybrid integrated photonics[4] and showcases the prospects of the III−V grown on Si platform. Based on the results achieved by 1.3 μm QD lasers
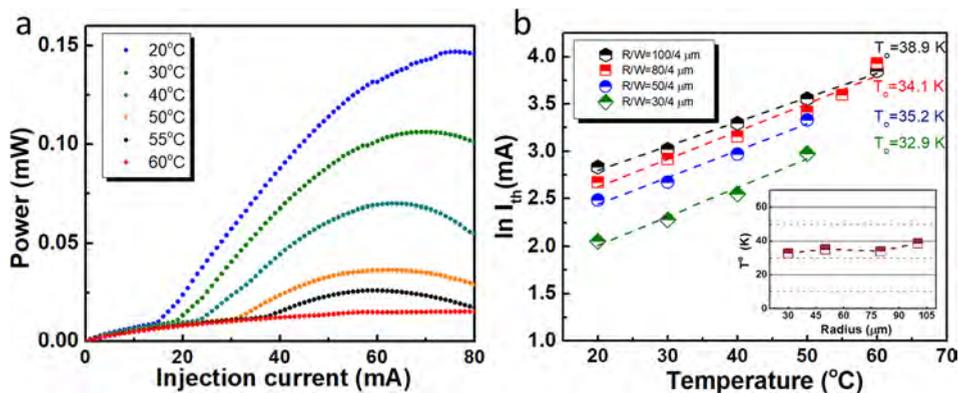
**Figure 6.** (a) Microring laser with a radius of 100 $\mu$m and ring width of 4 $\mu$m shows continuous-wave lasing up to 55 °C. (b) Plots of threshold current versus stage temperature for four different laser devices with various outer-ring radii. Inset: extracted characteristic temperature $T_0$ as a function of outer-ring radius.
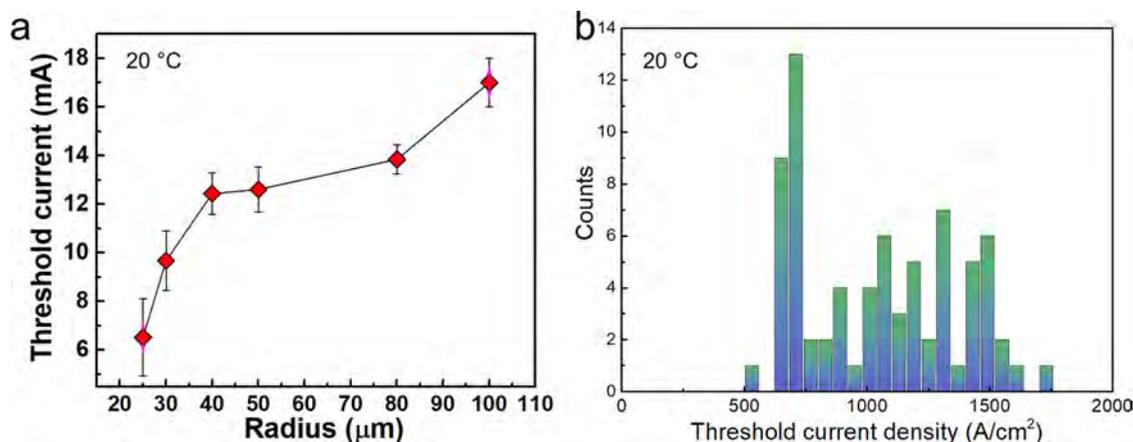


**Figure 7.** (a) Room-temperature continuous-wave threshold currents for 74 measured lasers of various cavity sizes. Bars represent standard deviation. (b) Corresponding histogram of CW threshold current density of these devices.

grown on Si, we expect 1.55 $\mu$m QDash lasers to show high immunity to crystalline defects from heteroepitaxial growth.[37] Furthermore, since Shockley-Read-Hall recombination in InP related compounds is less severe than in GaAs,[38] longer operating lifetimes are expected compared with the state of the art GaAs-based devices epitaxially grown on Si.[39]

Still, the total output power in the lateral direction of the ring cavity is relatively low compared to conventional linear cavity lasers. The anisotropy of gain with respect to QDash elongation orientation[40] impacts the fullest exploitation of QDash gain in a microring laser device, which, in turn, would affect the output power and the performance characteristics. Furthermore, the measured optical power was collected through the radiation out-coupling from one side of the cavity. This is only a small fraction of the total power considering the angular directivity pattern of radiation. In this regard, advanced device implementation methods such as using nanoantennas,[41] waveguide-coupled microspiral,[42,43] deformed microcavities,[44] vertical coupling into a silicon-on-insulator waveguide via bonding,[4,45] lateral evanescent coupling to a straight waveguide,[46] and so on can be used to improve outcoupling efficiency from the WGM microcavity. Second, an improved active region design of QDash-in-a-well with better carrier confinement can be used to enhance the total optical power of the QDash microring lasers, which has shown better performance in linear cavity lasers.[47] This

includes, and is not limited to, utilization of variable barrier thickness InGaAlAs barrier in the multistack Qdash structure,[48] modifying shape, and composition of the quantum dashes by adjusting the nominal thickness,[49] optimization of optical gain properties through spatial arrangement, barrier widths, and QDash layer thicknesses.[50] Furthermore, these challenges become less acute in the course of applications requiring low output powers or sensitive photodetectors. For example, in ref 51, despite a low lateral free-space outcoupling efficiency, an electrically pumped micropost WGM microlaser can act as an integrated light source to optically excite nearby microresonator structures for on-chip quantum optics experiments. In ref 52, triggered by a monolithically integrated on-chip QD WGM microlaser, tunable emission energy is achieved on a QD micropillar-based single-photon source. In ref 53, a microring laser was integrated with a photodetector sharing the same InAs/GaAs quantum dot active region. This enables efficient on-chip data transmission from the same epitaxial stack by directly driving the laser and applying a constant reverse bias voltage to the photodetector.

In addition to output power, another important aspect that worth consideration is the potential of this structured laser in single mode lasing. Most of the large rings have closely spaced high quality factor modes of different azimuthal orders and thus exhibit multimode lasing spectra and bistability. Although the suppression of nonradiative sidewall recombination effects

of Qdashes grant the feasibility of device miniaturization, which enforces single mode operation since FSR scales inversely with size. Mode management is still demanding because of the inhomogeneously broadened gain bandwidth, which will not prevent the neighboring resonances from also experiencing amplification. This can be achieved by integrating second order gratings on the microring waveguide,[54] harnessing notions from parity-time symmetry,[55] and extreme confinement of light in subwavelength structures using metallic cavities.[56] Additionally, a systematic study at the device level of the absolute power efficiency, lifetime, reliability, and reproducibility is needed to reduce the footprint further and enable larger scale on-chip integration.

## ■ AUTHOR INFORMATION

**Corresponding Author**
*E-mail: yatingwan@ucsb.edu.

**ORCID** ○
Yating Wan: 0000-0003-2157-2406

**Author Contributions**
‡These authors contributed equally to this work.

**Notes**
The authors declare no competing financial interest.

## ■ ACKNOWLEDGMENTS

## ■ REFERENCES

(1) Heck, M. J. R.; Bowers, J. E. Energy efficient and energy proportional optical interconnects for multi-core processors: Driving the need for on-chip sources. *IEEE J. Sel. Top. Quantum Electron.* **2014**, *20*, 332−343.

(2) He, L.; Özdemir, Ş. K.; Yang, L. Whispering gallery microcavity lasers. *Laser Photon Rev.* **2013**, *7*, 60−82.

(3) Yao, Z.; Wu, K.; Tan, B. X.; Wang, J.; Li, Y.; Zhang, Y.; Poon, A. W. Integrated Silicon Photonic Microresonators: Emerging Technologies. *IEEE J. Sel. Top. Quantum Electron.* **2018**, *24*, 5900324.

(4) Liang, D.; Fiorentino, M.; Okumura, T.; Chang, H.-H.; Spencer, D. T.; Kuo, Y.-H.; Fang, A. W.; Dai, D.; Beausoleil, R. G.; Bowers, J. E. Electrically-pumped compact hybrid silicon microring lasers for optical interconnects. *Opt. Express* **2009**, *17*, 20355−20364.

(5) Fujita, M.; Inoshita, K.; Baba, T. Room temperature continuous wave lasing characteristics of GaInAsP/InP microdisk injection laser. *Electron. Lett.* **1998**, *34*, 278−279.

(6) Krauss, T.; Laybourn, P. J. R.; Roberts, J. CW operation of semiconductor ring lasers. *Electron. Lett.* **1990**, *26*, 2095−2097.

(7) Kryzhanovskaya, N. V.; Maximov, M. V.; Zhukov, A. E. Whispering-gallery mode microcavity quantum-dot lasers. *Quantum Electron.* **2014**, *44*, 189.

(8) Wan, Y.; Norman, J.; Li, Q.; Kennedy, M.; Liang, D.; Zhang, C.; Huang, D.; Zhang, Z.; Liu, A.; Torres, A.; Jung, D.; Gossard, A.; Hu, E.; Lau, K.; Bowers, J. 1.3 μm submilliamp threshold quantum dot micro-lasers on Si. *Optica* **2017**, *4*, 940−944.

(9) Kryzhanovskaya, N. V.; Zhukov, A. E.; Maximov, M. V.; Moiseev, E. I.; Shostak, I. I.; Nadtochiy, A. M.; Kudashova, Y. V.; Lipovskii, A. A.; Kulagina, M. M.; Troshkov, S. I. Room temperature lasing in 1-μm microdisk quantum dot lasers. *IEEE J. Sel. Top. Quantum Electron.* **2015**, *21*, 709.

(10) Wan, Y.; Li, Q.; Liu, A. Y.; Gossard, A. C.; Bowers, J. E.; Hu, E. L.; Lau, K. M. Sub-wavelength InAs quantum dot micro-disk lasers epitaxially grown on exact Si (001) substrates. *Appl. Phys. Lett.* **2016**, *108*, 221101.

(11) Moiseev, E.; Kryzhanovskaya, N.; Maximov, M. V.; Zubov, F.; Nadtochiy, A. M.; Kulagina, M. M.; Zadiranov, Y.; Kalyuzhnyy, N.; Mintairov, S.; Zhukov, A. Highly efficient injection microdisk lasers based on quantum well-dots. *Opt. Lett.* **2018**, *43*, 4554.

(12) Wan, Y.; Inoue, D.; Jung, D.; Norman, J. C.; Shang, C.; Gossard, A. C.; Bowers, J. E. Directly modulated quantum dot lasers on silicon with a milliampere threshold and high temperature stability. *Photonics Res.* **2018**, *6*, 776−781.

(13) Bhowmick, S.; Baten, M. Z.; Frost, T.; Ooi, B. S.; Bhattacharya, P. High performance InAs/In$_{0.53}$Ga$_{0.23}$Al$_{0.24}$AsInP quantum dot 1.55 μm tunnel injection laser. *IEEE J. Quantum Electron.* **2014**, *50*, 7−14.

(14) Khan, M. Z. M.; Ng, T. K.; Ooi, B. S. Self-assembled InAs/InP quantum dots and quantum dashes: Material structures and devices. *Prog. Quantum Electron.* **2014**, *38*, 237−313.

(15) Wang, R. H.; Stintz, A.; Varangis, P. M.; Newell, T. C.; Li, H.; Malloy, K. J.; Lester, L. F. Room temperature operation of InAs quantum-dash lasers on InP [001]. *IEEE Photonics Technol. Lett.* **2001**, *13*, 767−769.

(16) Schwertberger, R.; Gold, D.; Reithmaier, J. P.; Forchel, A. Long-wavelength InP-based quantum-dash lasers. *IEEE Photonics Technol. Lett.* **2002**, *14*, 735−737.

(17) Sadeev, T.; Arsenijević, D.; Bimberg, D. Comparison of dynamic properties of InP/InAs quantum-dot and quantum-dash lasers. *Appl. Phys. Lett.* **2016**, *109*, 161104.

(18) Hein, S.; Podemski, P.; Sęk, G.; Misiewicz, J.; Ridha, P.; Fiore, A.; Patriarche, G.; Höfling, S.; Forchel, A. Orientation dependent emission properties of columnar quantum dash laser structures. *Appl. Phys. Lett.* **2009**, *94*, 241113.

(19) Rotter, T.; Stintz, A.; Malloy, K. InP based quantum dash lasers with 2 μm wavelength. *IEE Proc.: Optoelectron.* **2003**, *150*, 318−321.

(20) Mrowiński, P.; Tarnowski, K.; Olszewski, J.; Somers, A.; Kamp, M.; Reithmaier, J. P.; Urbańczyk, W.; Misiewicz, J.; Machnikowski, P.; Sęk, G. Tailoring the photoluminescence polarization anisotropy of a single InAs quantum dash by a post-growth modification of its dielectric environment. *J. Appl. Phys.* **2016**, *120*, 074303.

(21) Hurtado, A.; Nami, M.; Henning, I. D.; Adams, M. J.; Lester, L. F. Bistability patterns and nonlinear switching with very high contrast ratio in a 1550 nm quantum dash semiconductor laser. *Appl. Phys. Lett.* **2012**, *101*, 161117.

(22) Ooi, B. S.; Djie, H. S.; Wang, Y.; Tan, C. L.; Hwang, J. C.; Fang, X. M.; Fastenau, J. M.; Liu, A. W. K.; Dang, G. T.; Chang, W. H. Quantum dashes on InP substrate for broadband emitter applicationsIEEE. *IEEE J. Sel. Top. Quantum Electron.* **2008**, *14*, 1230−1238.

(23) Khan, M. Z. M.; Ng, T. K.; Lee, C. S.; Bhattacharya, P.; Ooi, B. S. Chirped InAs/InP quantum-dash laser with enhanced broad spectrum of stimulated emission. *Appl. Phys. Lett.* **2013**, *102*, 091102.

(24) Capua, A.; Saal, A.; Karni, O.; Eisenstein, G.; Reithmaier, J. P.; Yvind, K. Complex characterization of short-pulse propagation through InAs/InP quantum-dash optical amplifiers: from the quasi-linear to the two-photon-dominated regime. *Opt. Express* **2012**, *20*, 347−353.

(25) Reithmaier, J. P.; Somers, A.; Deubert, S.; Schwertberger, R.; Kaiser, W.; Forchel, A.; Galligaro, M.; Resneau, P.; Parillaud, O.; Bansropun, S.; Krakowski, M.; Alizon, R.; Hadass, D.; Bilenca, A.; Dery, H.; Mikhelashvili, V.; Eisenstein, G.; Gioannini, M.; Montrosset, I.; Berg, T. W.; van der Poel, M.; Mork, J.; Tromborg, B. InP based lasers and optical amplifiers with wire-/dot-like active regions. *J. Phys. D: Appl. Phys.* **2005**, *38*, 2088−2102.

(26) Gosset, C.; Merghem, K.; Martinez, A.; Moreau, G.; Patriarche, G.; Aubin, G.; Ramdane, A. Subpicosecond pulse generation at 134 GHz using a quantum-dash-based Fabry-Perot laser emitting at 1.56 μm. *Appl. Phys. Lett.* **2006**, *88*, 241105.

(27) Panapakkam, V.; Anthur, A. P.; Vujicic, V.; Zhou, R.; Gaimard, Q.; Merghem, K.; Aubin, G.; Lelarge, F.; Viktorov, E. A.; Barry, L. P.; Ramdane, A. Amplitude and phase noise of frequency combs generated by single-section InAs/InP quantum-dash-based passively and actively mode-locked lasers. *IEEE J. Quantum Electron.* **2016**, *52*, 1−7.

(28) Cao, H.; Deng, H.; Ling, H.; Liu, C.; Smagley, V. A.; Caldwell, R. B.; Smolyakov, G. A.; Gray, A. L.; Lester, L. F.; Eliseev, P. G.; Osiński, M. Highly unidirectional InAs/InGaAs quantum-dot ring lasers. *Appl. Phys. Lett.* **2005**, *86*, 203117.

(29) Barbarin, Y.; Anantathanasarn, S.; Bente, E. A. J. M.; Oei, Y. S.; Smit, M. K.; Notzel, R. 1.55-$\mu$m range InAs−InP (100) quantum-dot Fabry−Pérot and ring lasers using narrow deeply etched ridge waveguides. *IEEE Photonics Technol. Lett.* **2006**, *18*, 2644−2646.

(30) Hill, M. T.; Anantathanasarn, S.; Zhu, Y.; Oei, Y. S.; Van Veldhoven, P. J.; Smit, M. K.; Notzel, R. InAs−InP (1.55-$\mu$m Region) Quantum-Dot Microring Lasers. *IEEE Photonics Technol. Lett.* **2008**, *20*, 446−448.

(31) Shi, B.; Zhu, S.; Li, Q.; Wan, Y.; Hu, E. L.; Lau, K. M. Continuous-wave optically pumped 1.55 $\mu$m InAs/InAlGaAs quantum dot microdisk lasers epitaxially grown on silicon. *ACS Photonics* **2017**, *4*, 204−210.

(32) Jung, D.; Ironside, D. J.; Bank, S. R.; Gossard, A. C.; Bowers, J. E. Effect of growth interruption in 1.55 $\mu$ m InAs/InAlGaAs quantum dots on InP grown by molecular beam epitaxy. *J. Appl. Phys.* **2018**, *123*, 205302.

(33) Zhou, L.; Bo, B.; Yan, X.; Wang, C.; Chi, Y.; Yang, X. Brief Review of Surface Passivation on III-V Semiconductor. *Crystals* **2018**, *8*, 226.

(34) Black, L. E.; Cavalli, A.; Verheijen, M. A.; Haverkort, J. E.; Bakkers, E. P.; Kessels, W. M. M. Effective Surface Passivation of InP Nanowires by Atomic-Layer-Deposited $Al_2O_3$ with POx Interlayer. *Nano Lett.* **2017**, *17*, 6287−6294.

(35) Ikku, Y.; Yokoyama, M.; Takenaka, M.; Takagi, S.; Ichikawa, O.; Hata, M. Propagation-Loss Reduction in InGaAsP Photonic-Wire Waveguides by InP and $Al_2O_3$ Passivation Layers. *ECIO 2012*, Florence, Italy, April 25−28, 2012, 2012.

(36) Ushigome, R.; Fujita, M.; Sakai, A.; Baba, T.; Kokubun, Y. GaInAsP microdisk injection laser with benzocyclobutene polymer cladding and its athermal effect. *Jpn. J. Appl. Phys.* **2002**, *41*, 6364.

(37) Nishi, K.; Takemasa, K.; Sugawara, M.; Arakawa, Y. Development of quantum dot lasers for data-com and silicon photonics applications. *IEEE J. Sel. Top. Quantum Electron.* **2017**, *23*, 1−7.

(38) Fang, S. F.; Adomi, K.; Iyer, S.; Morkoc, H.; Zabel, H.; Choi, C.; Otsuka, N. Gallium arsenide and other compound semiconductors on silicon. *J. Appl. Phys.* **1990**, *68*, R31−R58.

(39) Jung, D.; Zhang, Z.; Norman, J.; Herrick, R.; Kennedy, M. J.; Patel, P.; Turnlund, K.; Jan, C.; Wan, Y.; Gossard, A. C.; Bowers, J. E. Highly reliable low-threshold InAs quantum dot lasers on on-axis (001) Si with 87% injection efficiency. *ACS Photonics* **2018**, *5*, 1094−1100.

(40) Ukhanov, A. A.; Wang, R. H.; Rotter, T. J.; Stintz, A.; Lester, L. F.; Eliseev, P. G.; Malloy, K. J. Orientation dependence of the optical properties in InAs quantum-dash lasers on InP. *Appl. Phys. Lett.* **2002**, *81*, 981−983.

(41) Moiseev, E. I.; Kryzhanovskaya, N.; Polubavkina, Y. S.; Maximov, M. V.; Kulagina, M. M.; Zadiranov, Y. M.; et al. Light Outcoupling from Quantum Dot-Based Microdisk Laser via Plasmonic Nanoantenna. *ACS Photonics* **2017**, *4*, 275−281.

(42) Yang, Y. D.; Zhang, Y.; Huang, Y. Z.; Poon, A. W. Direct-modulated waveguide-coupled microspiral disk lasers with spatially selective injection for on-chip optical interconnects. *Opt. Express* **2014**, *22*, 824−838.

(43) Shang, C.; Wan, Y.; Jung, D.; Norman, J.; Kennedy, M.; Liang, D.; Zhang, C.; Gossard, A. C.; Bowers, J. E. Quantum dot micro-lasers integrated with photodetectors and optical amplifiers on (001) Si via waveguide coupling. *CLEO: Science and Innovations*; Optical Society of America, 2018; SM2I. 6.

(44) Harayama, T.; Shinohara, S. Two dimensional microcavity lasers. *Laser. Photon. Rev.* **2011**, *5*, 247−271.

(45) Van Campenhout, J.; Rojo-Romeo, P.; Regreny, P.; Seassal, C.; Van Thourhout, D.; Verstuyft, S.; Di Cioccio, L.; Fedeli, J.; Lagahe, C.; Baets, R. Electrically pumped InP-based microdisk lasers integrated with a nanophotonic silicon-on-insulator waveguide circuit. *Opt. Express* **2007**, *15*, 6744−6749.

(46) Lv, X. M.; Huang, Y. Z.; Zou, L. X.; Long, H.; Du, Y. Optimization of direct modulation rate for circular microlasers by adjusting mode Q factor. *Laser. Photon. Rev.* **2013**, *7*, 818−829.

(47) Reithmaier, J. P.; Eisenstein, G.; Forchel, A. InAs/InP quantum-dash lasers and amplifiers. *Proc. IEEE* **2007**, *95*, 1779−1790.

(48) Khan, M. Z. M.; Ng, T. K.; Lee, C. S.; Bhattacharya, P.; Ooi, B. S. Investigation of chirped InAs/InGaAlAs/InP quantum dash lasers as broadband emitters. *IEEE J. Quantum Electron.* **2014**, *50*, 51−61.

(49) Sauerwald, A.; Kümmell, T.; Bacher, G.; Somers, A.; Schwertberger, R.; Reithmaier, J. P.; Forchel, A. Size control of InAs quantum dashes. *Appl. Phys. Lett.* **2005**, *86*, 253112.

(50) Somers, A.; Kaiser, W.; Reithmaier, J. P.; Forchel, A.; Gioaninni, M.; Montrosset, I. Optical gain properties of InAs/InAlGaAs/InP quantum dash structures with a spectral gain bandwidth of more than 300 nm. *Appl. Phys. Lett.* **2006**, *89*, 061107.

(51) Stock, E.; Albert, F.; Hopfmann, C.; Lermer, M.; Schneider, C.; Höfling, S.; Forchel, A.; Kamp, M.; Reitzenstein, S. On-Chip Quantum Optics with Quantum Dot Microcavities. *Adv. Mater.* **2013**, *25*, 707−710.

(52) Munnelly, P.; Heindel, T.; Thoma, A.; Kamp, M.; Höfling, S.; Schneider, C.; Reitzenstein, S. Electrically Tunable Single-Photon Source Triggered by a Monolithically Integrated Quantum Dot Microlaser. *ACS Photonics* **2017**, *4*, 790−794.

(53) Wan, Y.; Zhang, Z.; Chao, R.; Norman, J.; Jung, D.; Shang, C.; li, Q.; Kennedy, M.; Liang, D.; Zhang, C.; Shi, J. W.; Gossard, A. C.; Lau, K. M.; Bowers, J. E. Monolithically integrated InAs/InGaAs quantum dot photodetectors on silicon substrates. *Opt. Express* **2017**, *25*, 27715−27723.

(54) Arbabi, A.; Kamali, S. M.; Arbabi, E.; Griffin, B. G.; Goddard, L. L. Grating integrated single mode microring laser. *Opt. Express* **2015**, *23*, 5335−5347.

(55) Hodaei, H.; Miri, M. A.; Heinrich, M.; Christodoulides, D. N.; Khajavikhan, M. Parity-time−symmetric microring lasers. *Science* **2014**, *346*, 975−978.

(56) Feng, L.; Wong, Z. J.; Ma, R. M.; Wang, Y.; Zhang, X. Single-mode laser by parity-time symmetry breaking. *Science* **2014**, *346*, 972−975.

G